International Journal of Thermal Sciences 49 (2010) 680–691

Contents lists available at ScienceDirect

International Journal of Thermal Sciences

journal homepage: www.elsevier.com/locate/ijts

Determination of stagnation and convective zones in a solar cavity receiver

M. Prakash, S.B. Kedare, J.K. Nayak*

Department of Energy Science and Engineering, Indian Institute of Technology Bombay, Mumbai 400076, India

ARTICLE INFO

Article history:
Received 30 September 2008
Accepted 10 June 2009
Available online 13 September 2009

Keywords:
Parabolic dish-receiver systems
Cavity receiver
Convective zone
Stagnation zone
Air temperature gradient (ATG)
Critical air temperature gradient

ABSTRACT

The convective heat loss mechanism in a solar cavity receiver is influenced by the presence of the stagnation and convective zone within the receiver. This paper focuses on the experimental and numerical studies carried out to identify these zones in a downward facing cylindrical cavity receiver of length 0.5 m, internal diameter 0.3 m and having a wind skirt of 0.5 m in diameter. This design is different from the receiver used normally for dish-Stirling systems. It is meant for providing low and medium temperature process heat and does not have stringent constraints on tube volume and pressure drop. The experiments are conducted for low and medium fluid inlet temperatures between 50 °C and 150 °C for receiver inclination angles of 0 (side ways facing cavity), 30, 45, 60 and 90° (vertically downward facing receiver). Water is used as the working fluid within the receiver tubes during the low temperature tests (50–75 °C) while compressed air is the working fluid for the medium temperature tests (130 and 150 °C). The numerical investigations have also been carried out for various conditions. The air velocity and temperature profiles obtained from the numerical and experimental studies are analysed to determine the zone boundary, which is found to be nearly a horizontal plane passing through the topmost point of the cavity aperture. This validates the results reported in the literature. This paper proposes a quantitative estimate for identifying the zone boundary and a term called "critical air temperature gradient" is defined for this purpose. The locations within the cavity having the air temperature gradient less than the critical air temperature gradient represent the stagnation zone. The locations having air temperature gradient more than the critical air temperature gradient represent the convective zone. A non-dimensional parameter ψ is defined to represent the values of the air temperature gradient. It is observed that a value of about 0.3 for ψ corresponds to the critical air temperature gradient for all the tests carried out. The stagnation zone is observed at regions having $\psi \leq 0.3$ and convective zone having $\psi > 0.3$.

1. Introduction

Solar concentrators are used for many applications such as supplying process heat to industries, generating electricity, melting and processing of metals as in the case of solar furnaces, etc. Many varieties of concentrators are used in various parts of the world. Recently in India, Fresnel parabolic dish with a cavity receiver is being used for supplying low and medium temperature process heat (Kedare et al. [1]). It consists of a mirror assembly in the form of a dish and a cavity receiver with a helical metallic coil. Such a system does not need any evacuated tube construction and uses simple float glass mirrors as reflectors. This makes the system cheaper in Indian scenario and durable in industrial environments. Working fluids used in such systems are thermic oils, air or pressurized water. According to Harris and Lenz [2], the thermal and optical losses occurring from an open cavity solar receiver are less than that of other types of receivers and hence, such receivers are preferred. The current paper focuses on the investigations of stagnation and convective zone in these receivers. The temperature level of process heat targeted by such systems is around 100–200 °C, which corresponds to the mean fluid temperature (with inlet fluid as 30 °C) between 60 °C and 115 °C. This fluid mean temperature range has been covered in the current investigation.

The efficiency of the parabolic dish-receiver system is directly affected by the thermal losses taking place from the cavity receiver. Besides, there is reflection loss of the concentrated solar flux from the receiver. The thermal losses include convective and radiative loss to the air in the cavity and conductive heat loss through the insulation used behind the helical tube surface. Losses due to reflection from the absorber surface depend on the receiver coil and its view factors whereas the radiative and the conductive heat losses are dependent on the cavity wall temperature, the view factors and the insulation material. These losses are reported to be independent of the cavity inclination (Stine and McDonald [3]; Leibfried and Ortjohann [4]). In case of convective heat losses, the phenomenon is complex as the heat transfer is dependent on the

* Corresponding author. Tel.: +91 22 25767881; fax: +91 22 25764890.
E-mail address: jknayak@iitb.ac.in (J.K. Nayak).

1290-0729/$ – see front matter © 2009 Elsevier Masson SAS. All rights reserved.
doi:10.1016/j.ijthermalsci.2009.06.015

Nomenclature

ATG	air temperature gradient (°C/m)
B	body force per unit volume
E	enthalpy
H	height of the cavity receiver (m)
k	thermal conductivity (W/m k)
L_{max}	diagonal length of the receiver (m)
P	pressure (N/m^2)
T_{fi}	fluid inlet temperature (°C)
T_∞	ambient temperature (°C)
ΔL	vertical distance between topmost point of cavity and thermocouple position (m)
ΔL_{zb}	maximum vertical distance from topmost point of cavity to the zone boundary (m)
ΔT	temperature difference between fluid inlet temperature and air temperature (°C)
$\Delta T/\Delta L$	air temperature gradient (°C/m)
u	velocity vectors
θ	cavity receiver inclination with respect to horizontal (degrees)
ρ	density (kg/m^3)
ψ	non-dimensional parameter described in Eq. (5)

air temperature and air velocities within the cavity which in turn is dependent on the inclination of the cavity, receiver temperatures, shape and size of the receiver and the external wind conditions (Clausing [5,6]).

Extensive studies on convective losses from cubical and rectangular open cavities have been reported (Le Quere et al. [7,8]; Penot [9]; Hess and Henze [10]; Chen et al. [11]; Chan and Tien [12,13]; Pavlovic and Penot [14]; Skok et al. [15]; Chakroun et al. [16]). In these studies, the cavity walls are either uniformly heated or one wall is heated and others are maintained in adiabatic condition. The presence of stagnation and convective zones has not been reported in these studies. The results of these studies cannot be directly extended to solar cavity receivers due to the fact that solar cavity receivers used with parabolic dish concentrators for low and medium temperature applications are mainly cylindrical in shape and the receiver walls have non-uniform temperatures. Besides, the analysis of different zones within the cavity is not explicitly made in these studies.

Clausing [5,6] proposed that the cavity receiver used for solar energy conversion devices can be divided into two zones namely a stagnation zone and a convective zone. The convective loss occurs from the convective zone and varies inversely with the stagnation zone area. The zone boundary between the two zones is a horizontal plane passing through the topmost point of the cavity aperture. However, no experimental validation of the zones for various receiver inclinations and the criteria for determining the zone boundary has been reported by the author.

Ma [17] and McDonald [18] performed experimental studies on convective losses in a conical frustum-cylinder shaped receiver during wind and no-wind conditions respectively. The conical frustum covered nearly half the length of the receiver while the remaining length included the cylindrical and the aperture section. The ratio of aperture diameter to the cavity diameter (diameter of the cylindrical section) in the studies by Ma [17] and McDonald [18] varied between 0.24 and 1. Besides, there is no wind skirt. These studies involve determination of total and convective losses and their dependencies on inclination, receiver temperatures and aperture sizes. The studies of Ma [17] and McDonald [18] are based on the zone boundary assumption developed by Clausing [5,6]. Ma [17] has mentioned the presence of two zones within the receiver while McDonald [18] has reported the respective zone areas.

Eyler [19] and Sendhil Kumar and Reddy [20] have carried out 2-dimensional numerical analysis of convective losses in rectangular and hemispherical solar cavity receiver respectively. 3-dimensional numerical analysis of cylindrical receivers is carried out by Paitoonsurikarn and Lovegrove [21,22] and Paitoonsurikarn et al. [23]. Numerical studies pertaining to combined radiation and convective loss from a hemispherical cavity receiver has been carried out [24,25]. The wall temperatures in these studies are assumed to be isothermal. These investigations have been carried out on simplified geometries considering the receiver tubes as plain walls. Besides, no quantitative basis has been reported for identifying the stagnation and convective zone within the receiver.

The literature survey shows that the types of receivers investigated both experimentally and numerically are cubical, rectangular, cylindrical and hemispherical in shape. The cylindrical receivers do not have a wind skirt and the diameter of the receiver aperture is less than that of the cavity. The current investigation considers a cylindrical receiver having the ratio of aperture diameter to the cavity diameter greater than one. The larger aperture ensures that all the reflected rays from the dish are intercepted by the receiver tubes. Such a receiver is being used with a concentrator for supplying industrial process heat at Latur, India (Kedare et al. [1]). The current paper discusses an approach to characterize the zone boundary of a cylindrical receiver (with a wind skirt) by bringing about a relationship between the air temperatures and the geometrical distances within the receiver. The influence of receiver inclination and receiver temperature is studied. Besides, the velocity profiles are obtained from the simulation results generated by using Fluent software (Fluent Inc. [26]) and are used for determining the zone boundaries in the current investigation. The experimental and numerical results are compared and the agreement is quite satisfactory.

2. Description of the receiver

The receiver used in the current investigation is shown in Fig. 1. It is a helical tube of internal diameter 0.3 m and height 0.5 m. It has 39 turns along the height of the receiver and 9 turns each at the back wall and the wind skirt. The tube material is copper and has a diameter of 0.009 m. The coil pitch is 0.013 m. The coils are coated with polyurethane coating that can withstand temperatures up to 350 °C. A layer of mineral wool insulation (0.075 m thick) is provided on the outer side of the tube coils. It is supported by an aluminium foil on the tube side and has a cladding of aluminium on the external side.

This particular shape of the receiver is a scaled-down version of the receiver used in a parabolic dish-receiver system installed at Mahananda dairy, Latur, Maharashtra, India for supplying process heat (Kedare et al. [1]). The dimension of the receiver in the field is about 1.7 times that of the receiver analysed in this work. It has been proposed to install receivers having shape and size similar to the experimental receiver in future projects for process heat applications and hence this characterization work has been undertaken.

3. Experimental investigations

The experimental convective loss studies from a solar cavity receiver can be carried out either under the on-flux or off-flux mode. In the on-flux mode, the receiver is tested in actual solar conditions by placing it at the focus of a parabolic dish concentrator. In the present study the experiments are carried out under the off-flux mode. The temperature gradient inside the cavity similar to the

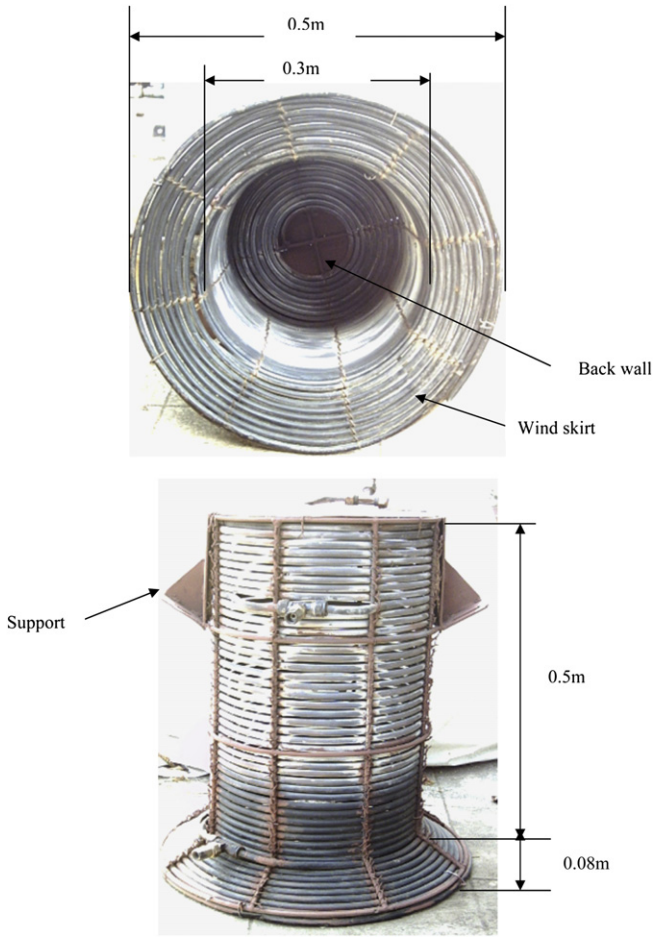

Fig. 1. Solar cavity receiver.

actual solar receiver is achieved by passing hot water and compressed air through the receiver tubes during the low and medium fluid inlet temperature tests respectively. The tests are carried out in a controlled environment.

3.1. Experimental set-up

The schematic and the photograph of the experimental set-up for the low temperature tests (50–75 °C) is shown in Fig. 2. In these tests, water is used as the working fluid within the receiver tubes. It consists of a downward facing cylindrical cavity receiver supported by a stand so that it can be inclined at angles of 0°, 30°, 45°, 60° and 90° with respect to the horizontal. Water is used as the working fluid for convenience in these tests. A water tank of 125 L capacity having two heaters (total wattage of 3 kW) serves as the source of hot water. A 0.18 kW pump is used for circulating the water through the receiver tubes. The mass flow rate of hot water entering the receiver is measured with a rotameter. The temperatures of air in the cavity at 20 different locations and that of the fluid in the tube at five locations (including inlet and outlet) are measured. K-type thermocouples are used for all temperature measurements except the inlet. For better control, the inlet fluid temperature is measured by a Pt-100 RTD due to its increased stability. The ambient temperature is measured at a location not affected by the receiver temperatures. ADAM modules are used for data acquisition and the data is logged onto a computer using the ADAM View software. The hot water is circulated at constant inlet temperature through the receiver. The flow is kept constant for the complete period of an experimental run. The water exiting from the receiver flows back to the storage tank, making the system closed loop.

The experiments are also performed at medium fluid inlet temperatures (130 °C and 150 °C) using compressed air as the working fluid within the receiver tubes. The set-up for these tests consists of the receiver, a pressure regulator with an in-built air filter, an air heater, orifice plates with U-tube manometers for flow measurement, pressure gauges and valves for flow control. The schematic and photograph of the set-up is shown in Fig. 3. The working fluid in these tests is compressed air for convenience. A compressor of about 10 bar pressure and 0.040 kg/s mass flow rate is used as the source of compressed air. The pressure of the compressed air to the receiver is controlled by a pressure regulator. The impurities and moisture in the air is removed by an air filter, which is a part of the pressure regulator. Valves are used for flow control. The heater is made up of 3 heater coils, each having a capacity of 2 kW. The coils are arranged within a stainless steel body that can withstand pressures up to 25 bar. The power supplied to each heater coil is controlled by a variac. Orifice plates with U-tube manometers are used for measuring the airflow rates at the inlet to the heater and at the exit from the receiver.

All the measuring instruments used in the experiments are calibrated. Thermocouples and RTDs were calibrated with the help of standard which in turn was calibrated at ERTL (Electronic Regional Test Laboratory) West Zone, Mumbai, India. The rotameter and the orifice plates are calibrated in the laboratory itself. The thermocouples have an uncertainty of about ±0.5% for measurements between 50 °C and 150 °C, uncertainty in the RTD reading is about ±0.3% for 50–75 °C measurement. The rotameter had an uncertainty of about ±5% for 0.02 kg/s measurement while the orifice plates had an uncertainty of about ±5% for 0.006 kg/s measurement.

3.2. Experimental procedure

Hot water is used as working fluid and experiments with different inlet temperatures between 50 °C and 75 °C at various receiver inclinations have been carried out. The hot water enters the receiver at the topmost portion of the cavity and exits out from the lower most portion, near the wind skirt as shown in Fig. 2. This is to ensure that there is highest temperature at the top of the cavity receiver and lowest temperatures near the aperture similar to that during the actual operation of the receiver. The water flow rate is kept constant at 0.02 kg/s. In each test, the receiver inlet fluid temperature is maintained constant. The fluid temperatures and the tube temperatures are measured at intervals of 1 min and the experiment is continued till the outlet temperature remains steady for about half an hour. This signifies that the system has reached steady state. The corresponding cavity air temperatures are recorded only at steady state. The steady state is achieved for each test in about 3 h.

The procedure for the medium fluid inlet temperature tests is similar to the low temperature tests except that the compressed air is introduced as the working fluid into the receiver at about 5 bar pressure and a mass flow rate of 0.006 kg/s. Here the test is an open loop system as the air is not circulated back. The experiments are carried out for different inclinations under no-wind conditions. The steady state in these tests is achieved in about 1 h.

4. Numerical investigations

Numerical investigations are carried out using a 3-D CFD numerical model of the cavity receiver. Only the fluid inlet temperature and the fluid mass flow rate are given as inputs to the

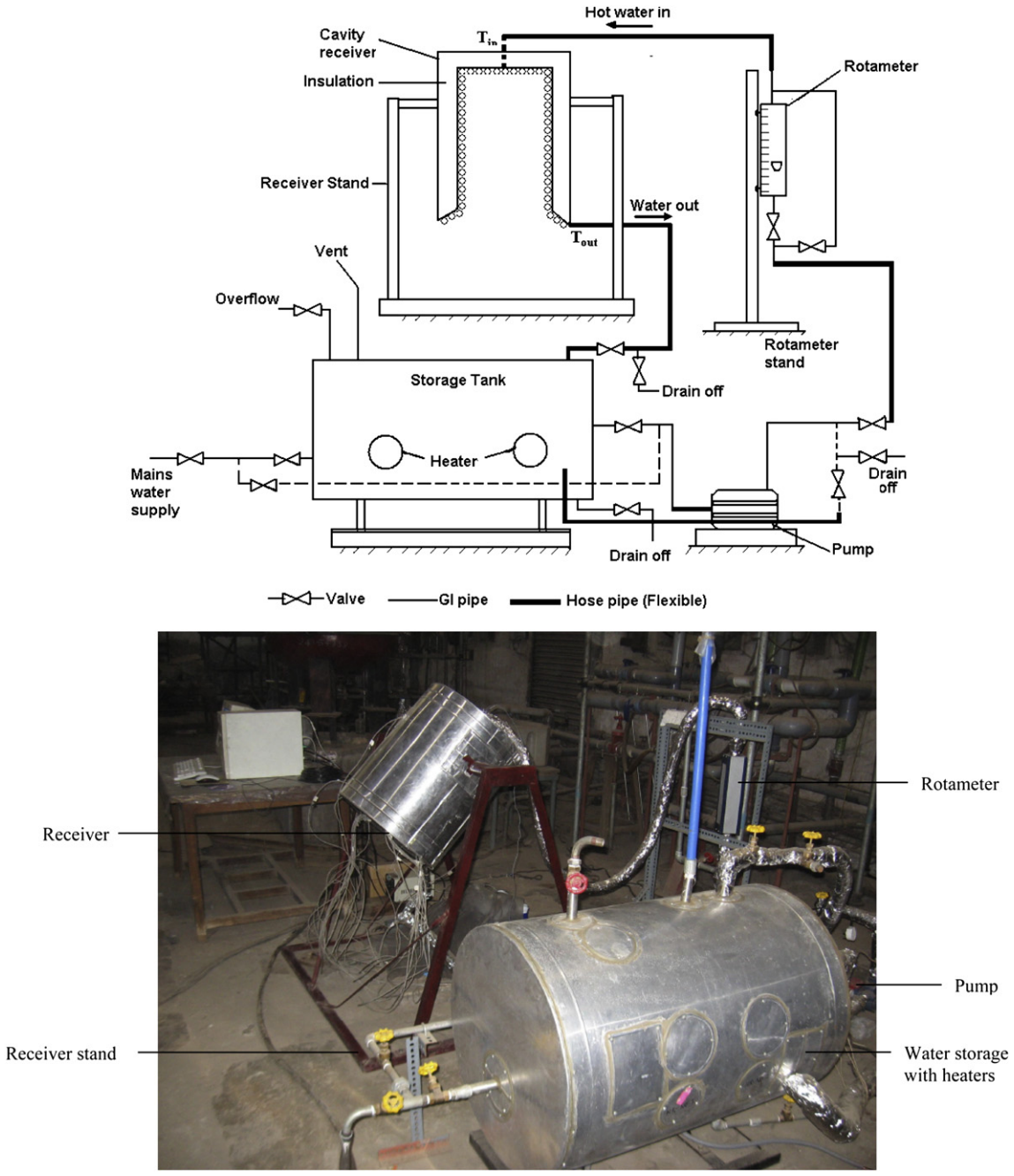

Fig. 2. Schematic and photograph of the low temperature experimental set-up.

simulation apart from the ambient temperature. The studies are limited to no-wind cases.

A helical coil (Fig. 4a) representing the cavity receiver is generated by using the Gambit tool of the Fluent 6.1.22 software. The coil is enclosed within a layer of insulation thus completing the cavity assembly. For the model, the region outside the cavity is represented by a cylindrical enclosure having diameter and length about fifteen times the receiver aperture diameter so that the airflow within the cavity is unaffected. The fluid inlet and the outlet tubes of the receiver are extended to the enclosure walls and are assumed to be adiabatic so that they do not affect the temperature and flow profile in the region external to the cavity. A fine mesh is used within the cavity including the tubes and the region between the receiver tubes and the insulation surface as shown in Fig. 4b. On the other hand, a coarse mesh is used for the region outside the cavity. The mesh progressively coarsens as the enclosure walls are approached from the cavity centre.

The material properties used for the simulation are taken from Holman [27]. The working fluid within the receiver tube for the low temperature test is water while compressed air is used for the medium temperature tests. On the other hand, the surrounding ambient air is considered to be present in the enclosure (Fig. 4b) and in the cavity interior. The Boussinesq approximation is made use of in the low temperature cases (50–75 °C) for the air properties. For higher inlet temperatures, the Boussinesq approximation is not used and ideal gas properties are used. This is due the limitations of the Boussinesq approximation as reported by Gray and Giorgini [28]. The boundary conditions used for the numerical

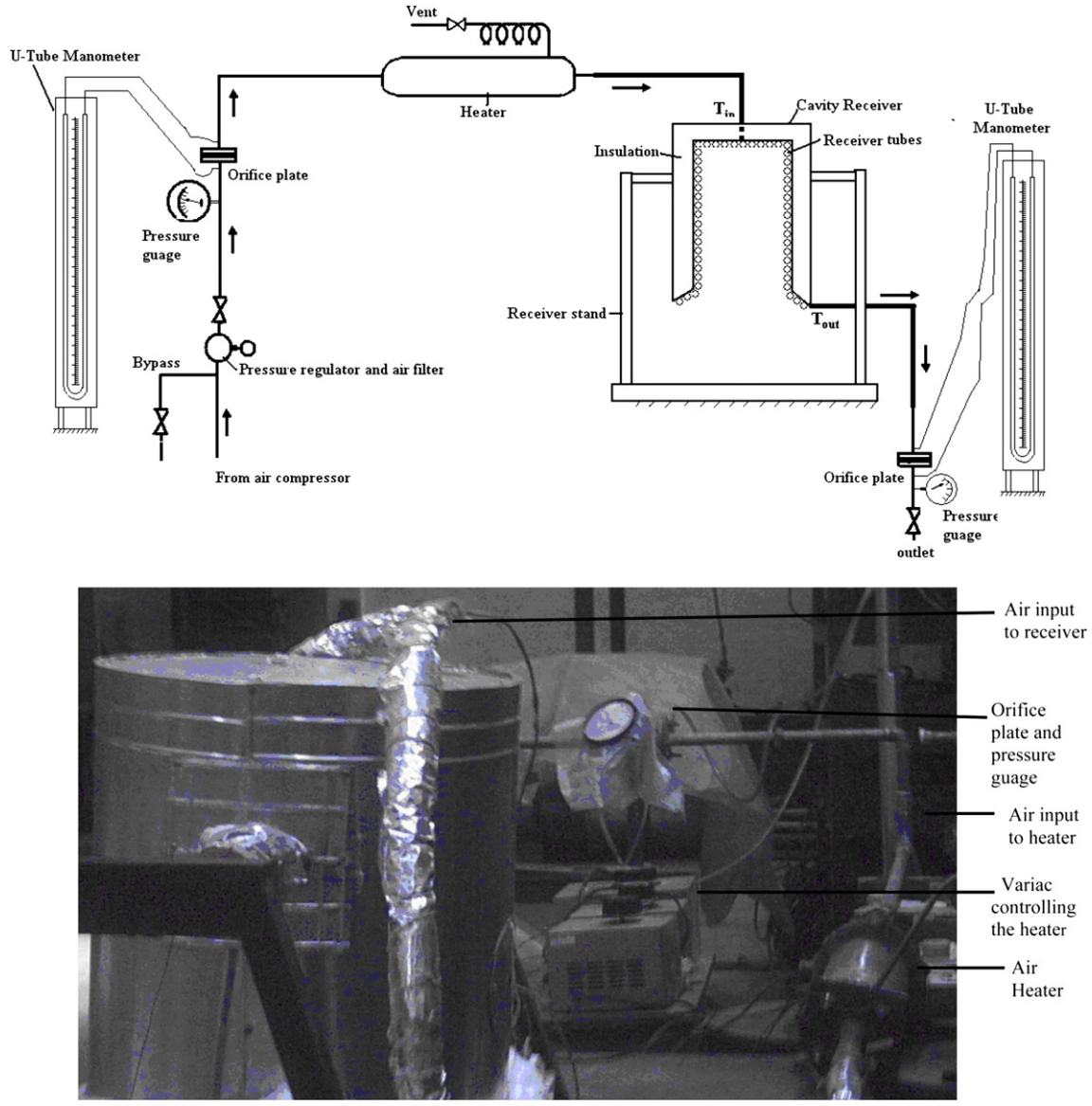

Fig. 3. Schematic and photograph of the medium temperature test set-up.

analysis are: (i) the fluid inlet temperature at the actual receiver outlet and the fluid velocity, (ii) adiabatic condition for the insulation surface and (iii) enclosure walls are maintained at ambient.

The solutions are obtained by solving the continuity equation, the momentum equation and the energy equation simultaneously. The basic equations used are

$$\nabla u = 0 \tag{1}$$

$$u\nabla u = B - \frac{\nabla P}{\rho} + \nu\nabla^2 u \tag{2}$$

$$\rho\frac{DE}{Dt} = \nabla(k\nabla T) + \frac{DP}{Dt} \tag{3}$$

The Semi-Implicit Pressure Linked Equation (SIMPLE) scheme of the Fluent software is used. It involves a pressure–velocity coupling and is used with a segregated solver for steady state problems. The momentum and energy solution controls are of the first order upwind type. The convergence criteria for the residuals of continuity and the velocity equations are of the order of 10^{-3} while for the energy equation it is 10^{-6}. The solutions are obtained once the convergence criteria are satisfied.

5. Results and discussion

The results obtained from the numerical simulation of the cavity receiver include the air temperature and velocity profiles within the receiver. Fig. 5 shows the typical velocity profiles at different inclinations for fluid inlet temperatures of 75 °C. The lowest velocity is represented by dark blue shade while the highest velocity is represented by the red shades. The shades green, yellow and orange lie between the blue and red shades. The region having velocities equal to or less than 15% of the air velocity of the surroundings is considered as the stagnation zone. Higher velocities refer to the movement of air mass and hence the region showing higher velocities is interpreted as convective zone. In addition there can be counter current pockets not connected to any region. These are not considered as convective zone as they do not indicate convective heat loss to the outside ambient. It can be noticed that the maximum velocity within the receiver at the 90°

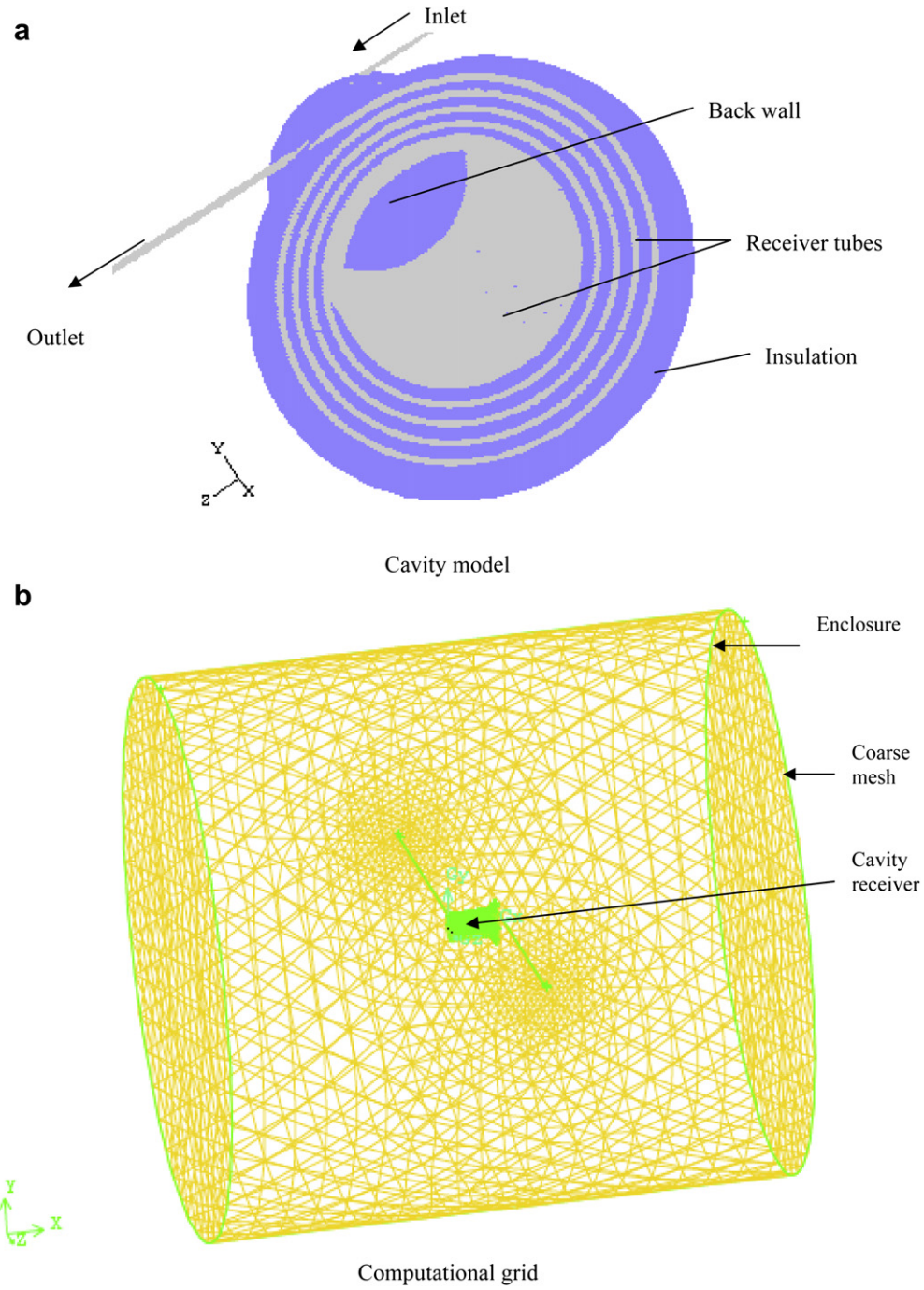

Fig. 4. (a) and (b) Cavity model and the grid used for numerical analysis.

inclination for the 75 °C fluid inlet temperature is about 0.04 m/s while the highest air velocity surrounding the receiver is about 0.25 m/s. The corresponding values for 45° inclination are 0.05 m/s and 0.4 m/s. Thus, it is seen that certain portions of the cavity have very low air velocities when compared to air velocities of the surroundings. At inclinations of 90°, the shift from the low velocity region to high velocity region is observed at the edges of the receiver aperture. The boundary between the stagnation and convective zones is termed as zone boundary where a sudden change in local air velocity is observed. At 0° inclination it can be seen that the velocities within the receiver are high though localized low velocity regions are observed very close to the back wall region of the receiver. A zone boundary is absent for 0° inclination as the condition for stagnation zone formation is not satisfied at majority of the locations within the receiver. Similar trends are observed for all fluid inlet temperatures.

The temperature profiles obtained from the numerical study at different inclinations for 75 °C, fluid inlet temperatures are shown in Fig. 6. The highest temperatures are depicted by the red shades and blue shades depict lowest temperatures. It can be seen from the temperature profiles that the regions depicted as stagnation zone from the velocity analysis have high air temperatures and are represented by the red shades while the convective zone has lower temperatures represented by yellow, green and blue

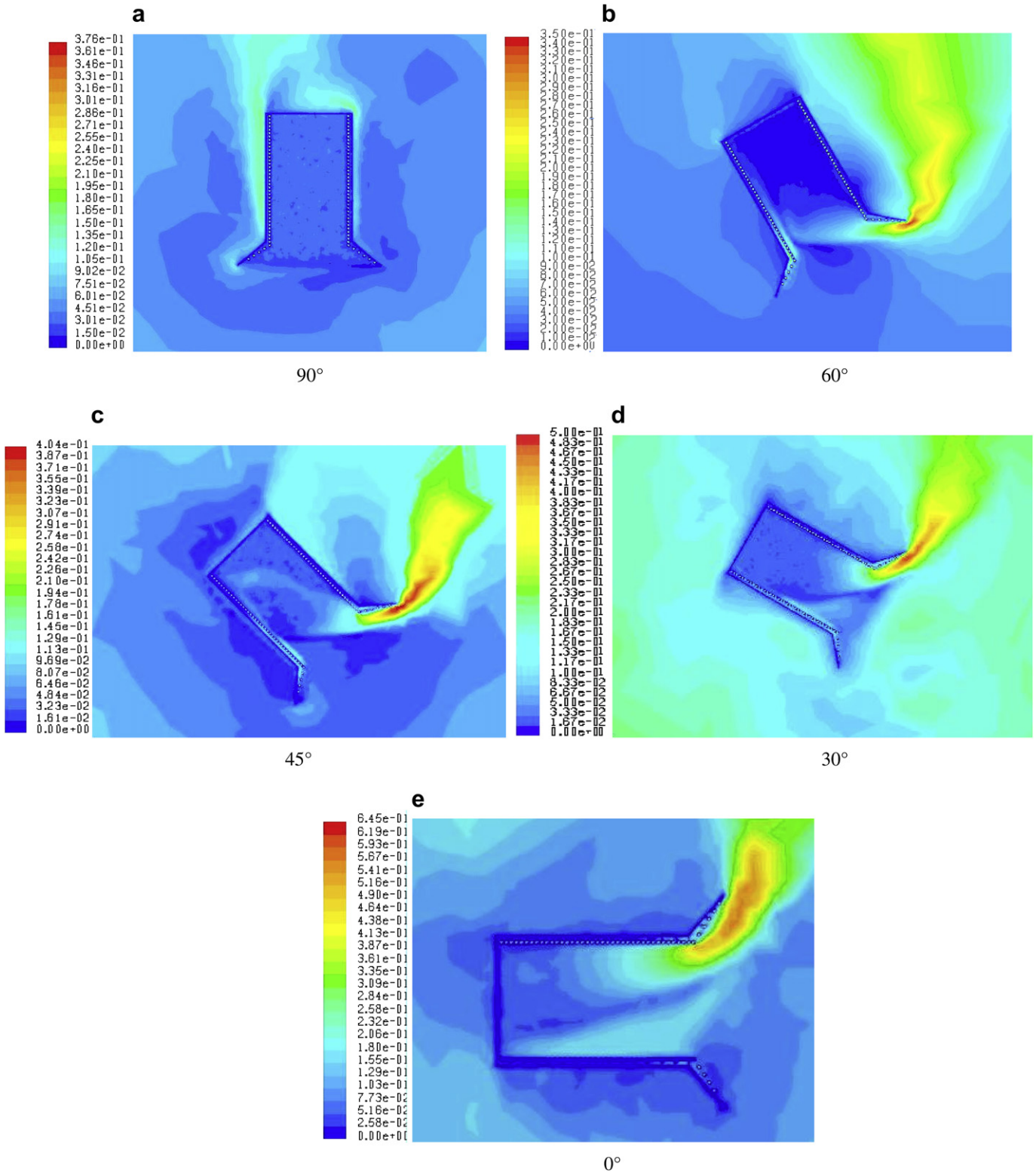

Fig. 5. Velocity profiles for 75° fluid inlet temperature at different inclinations (values are in m/s).

shades. The exception to this is the 0° inclination where the stagnation zone is absent and high air temperatures are observed at locations having high air velocities. The absence of stagnation zone allows the air to flow across the entire length of the receiver picking up heat from the receiver tubes. This increases the temperature of the outgoing air near the upper portions of the receiver. Similar results are obtained for all fluid inlet temperatures analysed. The zone boundary observed in Fig. 6 at 90°, 60°, 45° and 30° receiver inclinations can be approximated as a horizontal plane passing through the topmost point of the receiver aperture. This is similar to the results reported by Clausing [5,6], Ma [17] and McDonald [18].

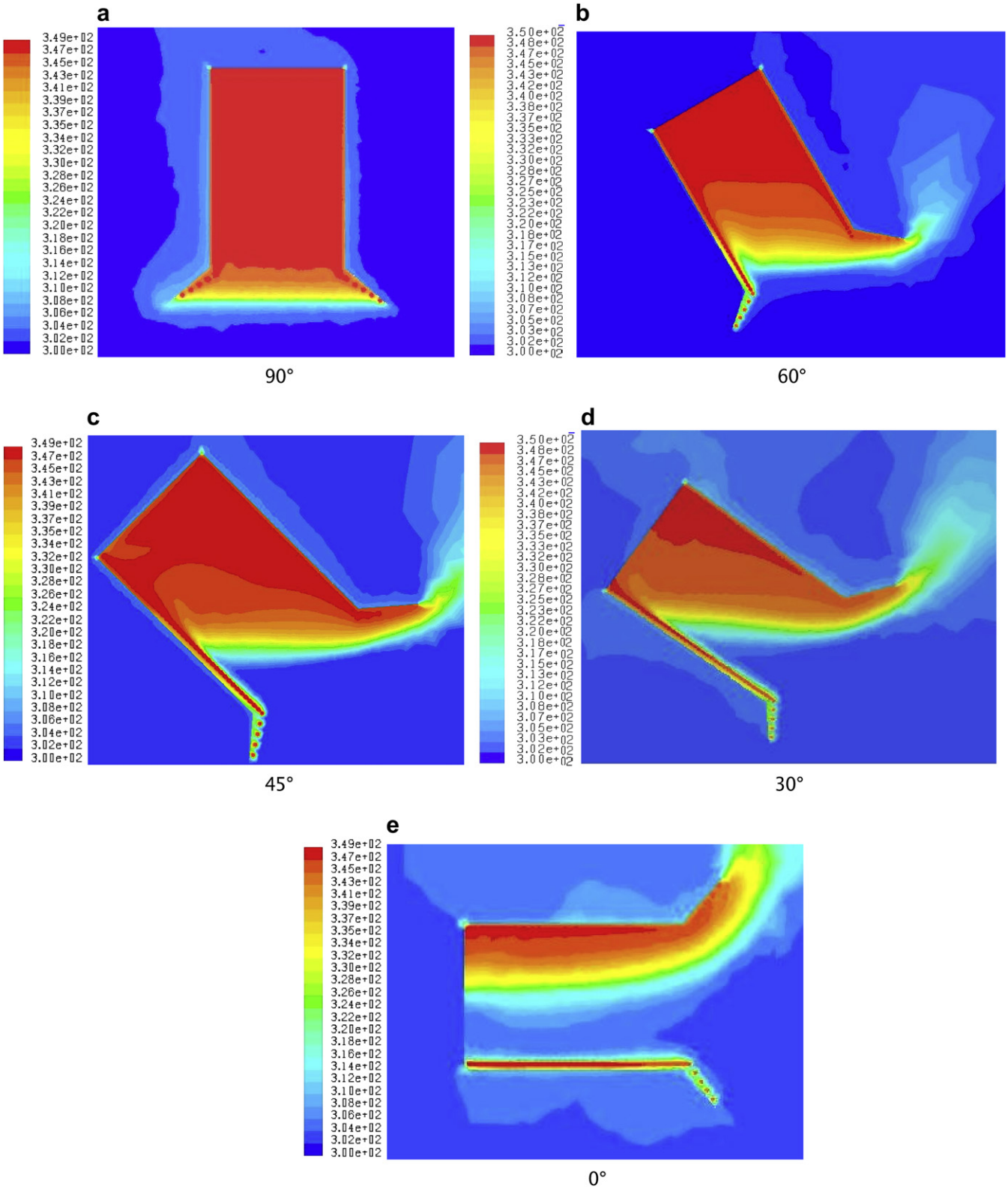

Fig. 6. Temperature profile for 75 °C fluid inlet temperature at different inclination angles (values are in Kelvin).

Table 1
Sample test results for 45° inclination at fluid inlet temperature of 75 °C.

ΔL (m)	T_{air} (°C)
0.10	75.00
0.10	75.00
0.10	74.70
0.10	74.80
0.20	75.00
0.20	75.00
0.20	74.80
0.20	73.80
0.30	74.10
0.30	74.10
0.30	74.10
0.30	72.90
0.40	71.00
0.40	71.00
0.40	70.60
0.40	70.60
0.45	68.25
0.45	67.80
0.45	66.90
0.45	66.00

$T_\infty = 30$ °C.
Mass flow rate of water = 0.02 kg/s.

The temperatures of air in the cavity are measured at 20 different locations. A sample test result is shown in Table 1. The difference of temperature between the fluid inlet temperature and the air temperature at any particular location within the receiver is calculated and is designated as ΔT. The vertical position of that location from the topmost point of the receiver (from the back wall side) is measured and this value is designated as ΔL as shown in Fig. 7. The air temperature gradient (ATG) is defined as

$$\text{Air Temperature Gradient (ATG)} = \frac{\Delta T}{\Delta L} \tag{4}$$

These values for different inclinations at fluid inlet temperatures 50, 60, 75, 130 and 150 °C are plotted in Figs. 8–11 respectively. The maximum uncertainty in the estimation of air temperature gradient is about 3 °C/m. Figs. 8–11 also show the air temperature gradients obtained numerically. The trends of the experimental and numerical results are similar, though the magnitudes of the former are higher. This is because the numerical simulations are only based on the convective losses but in experiments, in addition to convection there is also a certain degree of radiation and conduction losses as reported by Prakash et al. [29]. It is seen from Figs. 8–11 that the values of ATG change very slowly with ΔL for low

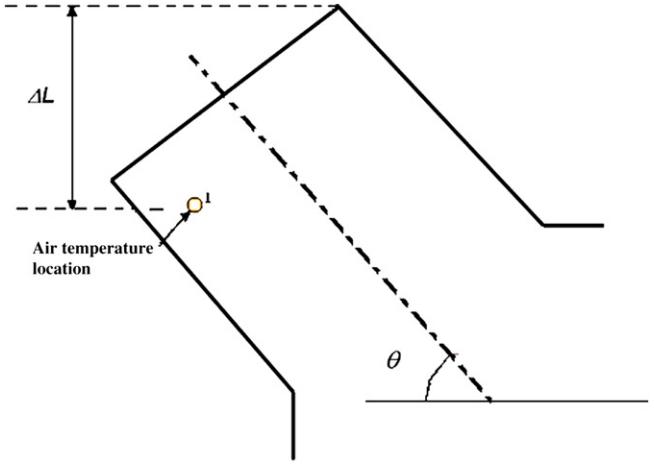

Fig. 7. Receiver inclined at an angle θ.

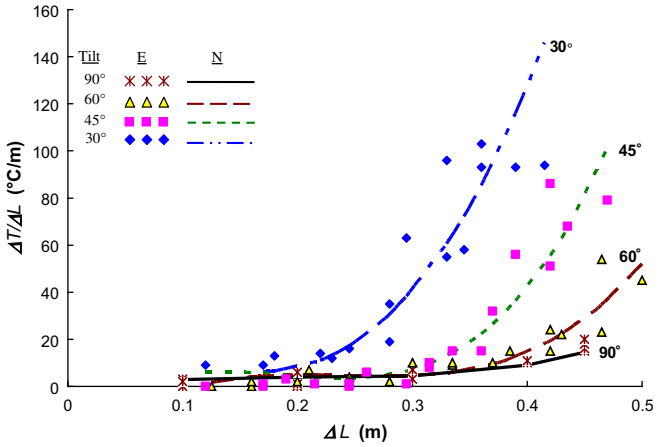

Fig. 8. ATG values at 75 °C fluid inlet temperature for different inclinations (E: Experimental, N: Numerical).

values of ΔL. However, after a certain value of ΔL, there is a sudden increase in the ATG values. This transition region is considered as the zone boundary and the corresponding ATG value is defined as the "critical air temperature gradient". It may be mentioned that the sudden increase in the values of ATG beyond the critical value is due to the decrease in air temperatures at those distances which indicates the formation of convective currents. This trend is observed at all inclinations except 0° receiver angle. It is found from Figs. 8–10 that the zone boundary at fluid inlet temperatures between 50 °C and 75 °C corresponds to a critical air temperature gradient of about 16–20 °C/m. It can be seen from Fig. 11 that the critical air temperature gradient for 150 °C and 130 °C fluid inlet temperatures is about 75 °C/m and 55 °C/m respectively. It can be seen from Fig. 5 that locations having temperature gradient greater than the critical air temperature gradient correspond to regions having higher air velocities. It would thus be reasonable to state that the locations within the cavity having the temperature gradient less than the critical temperature gradient represent the stagnation zone and the locations having higher values represent the convective zone.

A non-dimensional parameter ψ is defined to represent the air temperature gradients for all fluid inlet temperatures and receiver inclinations. It is defined by dividing the local air temperature gradient ($\Delta T/\Delta L$) by the maximum average air temperature gradient ($(T_{fi} - T_\infty)/L_{max}$). The value of ψ is defined as

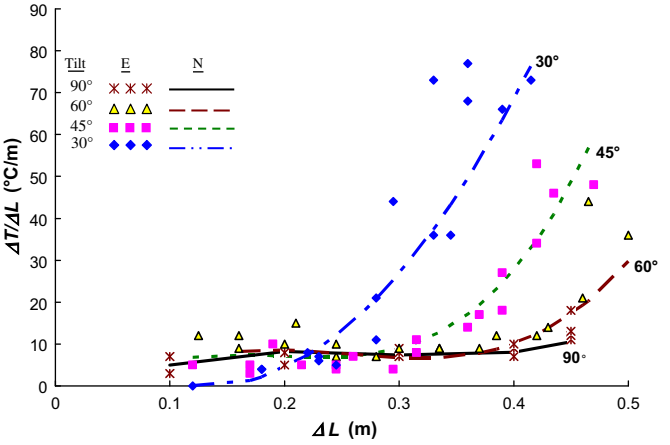

Fig. 9. ATG values at 60 °C fluid inlet temperature for different inclinations (E: Experimental, N: Numerical).

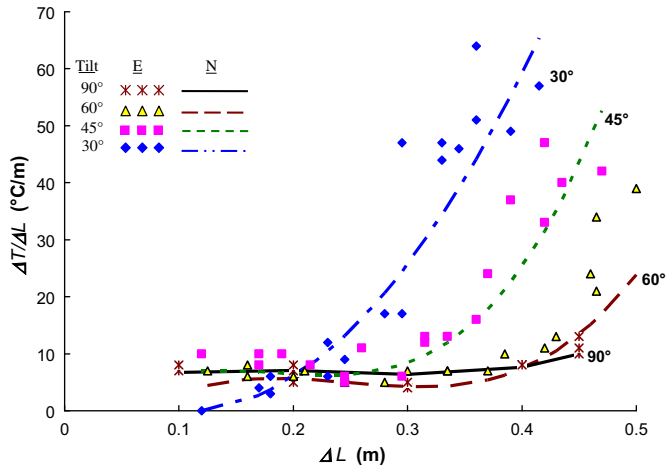

Fig. 10. ATG values at 50 °C fluid inlet temperature for different inclinations (E: Experimental, N: Numerical).

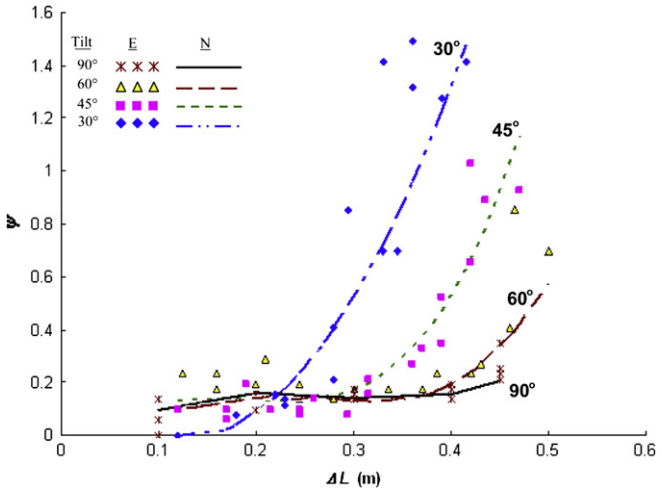

Fig. 13. Values of ψ at 60 °C fluid inlet temperature for different inclinations (E: Experimental, N: Numerical).

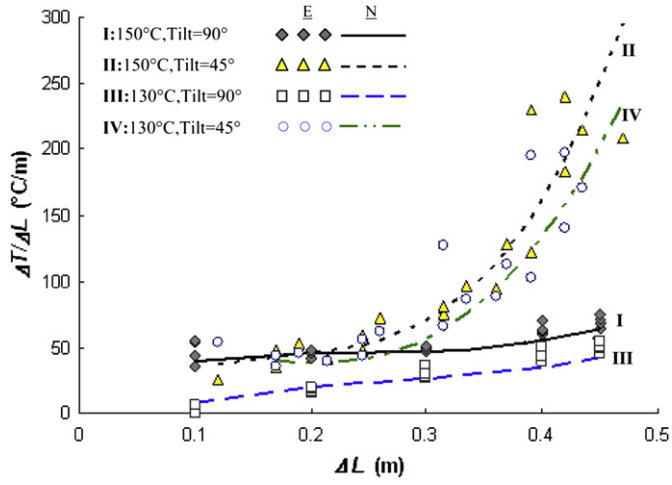

Fig. 11. ATG values at 150 °C and 130 °C fluid inlet temperature for 90° and 45° inclination (E: Experimental, N: Numerical).

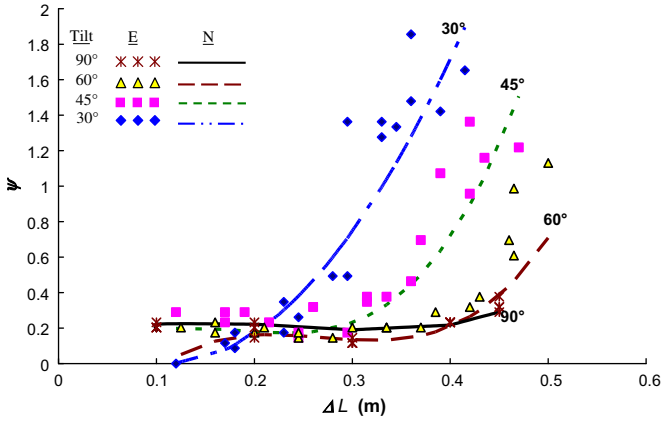

Fig. 14. Values of ψ at 50 °C fluid inlet temperature for different inclinations (E: Experimental, N: Numerical).

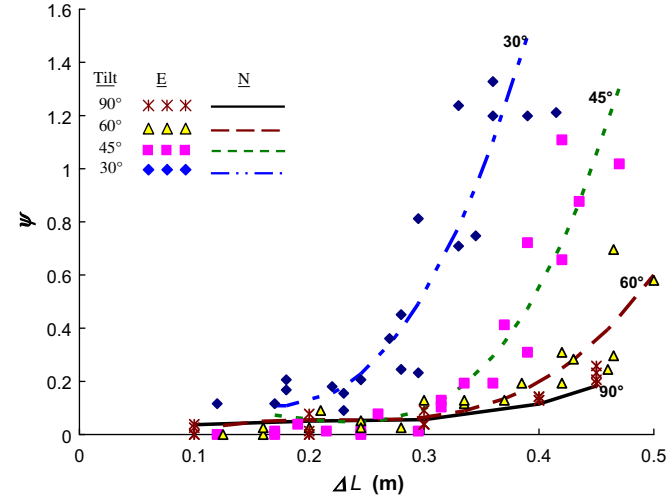

Fig. 12. Values of ψ at 75 °C fluid inlet temperature for different inclinations (E: Experimental, N: Numerical).

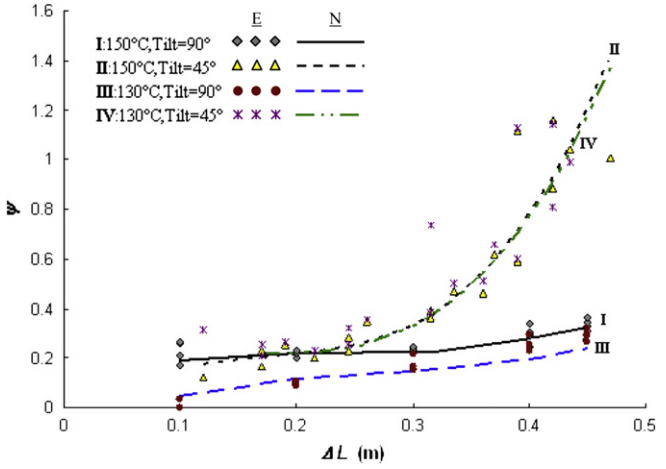

Fig. 15. Values of ψ at 150 °C and 130 °C fluid inlet temperature for different inclinations (E: Experimental, N: Numerical).

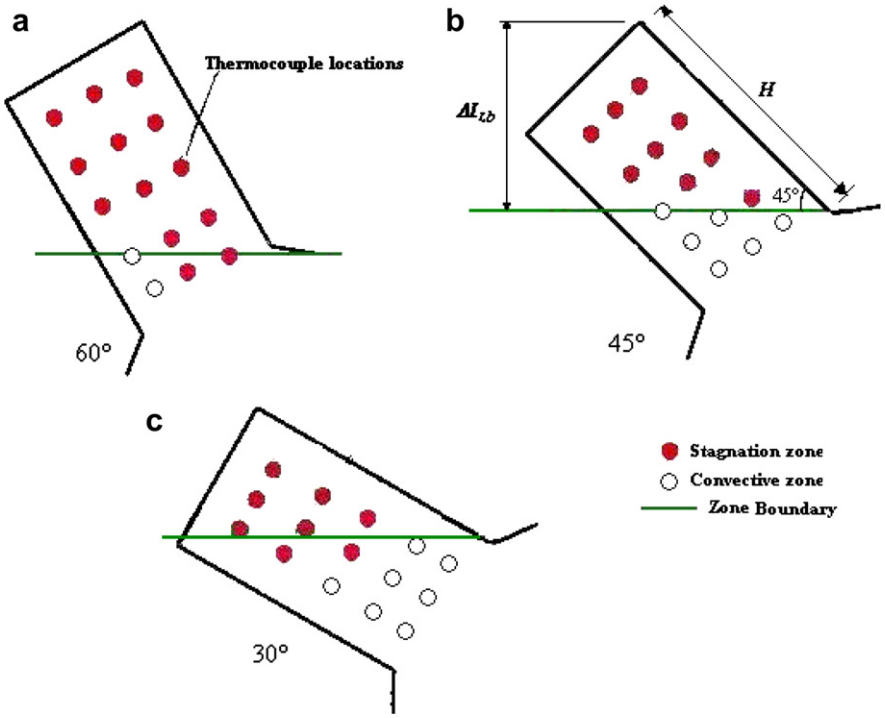

Fig. 16. Typical stagnation and convective zones for 60°, 45° and 30° inclination.

$$\psi = \frac{\Delta T}{\Delta L} \times \frac{L_{\max}}{(T_{\mathrm{fi}} - T_{\infty})} \tag{5}$$

where $(\Delta T/\Delta L)$ is the ATG value, $L_{\max}$ is the diagonal length of cavity receiver excluding the wind skirt, T_{fi} is the fluid inlet temperature and T_{∞} is the ambient temperature. The variations of ψ with ΔL for all fluid inlet temperatures investigated are shown in Figs. 12–15. It is observed from Figs. 12–15 that the non-dimensional air temperature gradient parameter (ψ) varies between 0 and 1.8 when inclinations between 90° and 30° are considered. It is seen that the critical air temperature gradient occurs at ψ of about 0.3. This is true for all receiver inclinations and fluid inlet temperatures tested in the current investigation. Stagnation zone corresponds to regions having $\psi \leq 0.3$ while the convective zone occurs at $\psi > 0.3$. For inclination of 0°, the value of ψ varies between 2 and 6, thus indicating that the stagnation zone is absent.

The zone boundary obtained from the experimental data is presented in Fig. 16 for inclinations of 60, 45 and 30° and is compared with that proposed by Clausing [5,6]. It is seen that a good agreement is observed between the two. Thus the zone boundary can be approximated as a horizontal plane passing through the topmost point of the receiver aperture. The relative areas of the stagnation and the convective zone are determined for the present cavity. It is observed that the convective zone covers about 5% of the entire cavity surface area at 90° inclination. At 60° inclination the convective zone covers about 28% of the cavity surface area while it is 44% and 55% at 45° and 30° inclination respectively. At 0° inclination, the convective zone covers the entire receiver area. This has direct effect on the convective losses from the cavity receiver of parabolic dish solar concentrators [29]. In the study carried out by Prakash et al. [29], the convective loss values obtained from the experimental and numerical analysis have been compared with those obtained using the Clausing approach [5,6]. It is noticed that there is a close agreement between the convective loss values with an average deviation of about 10%.

The knowledge of the air temperature at the zone boundary helps in estimating the convective loss from the receiver. This can be done from a knowledge of the value of ψ. It may be seen from Fig. 16 that the vertical distance from the topmost point of the receiver to the zone boundary (ΔL_{zb}) is $H\sin\theta$. This is known for a receiver of known height. Hence ΔT can be calculated from Eq. (5) since all the other parameters are know. Thus by estimating ψ for a particular condition (inclination and inlet fluid temperatures), the air temperature at the zone boundary can be calculated for all possible inclinations. This procedure can be adopted for any type of cavity receiver.

6. Conclusions

Experimental and numerical studies are carried out to identify the stagnation and convective zone in a downward facing cylindrical cavity receiver. The effects of fluid inlet temperature and receiver inclination angle are investigated. The following conclusions can be drawn:

(1) Air temperature and velocity profiles within the receiver studied experimentally and numerically under no-wind conditions indicate the existence of two zones. The experimental results on zone boundary is compared with that proposed by Clausing [5,6]. A good agreement is observed.
(2) A quantitative estimate for identifying the zone boundary has been proposed. A term called "critical air temperature gradient". The critical air temperature gradient obtained from the numerical results is in good agreement with the experimental values.
(3) A non-dimensional parameter ψ is defined to represent the values of the air temperature gradients. The value of the critical air temperature gradient corresponds to ψ of about 0.3 for all inclinations and all fluid inlet temperatures tested in the

current investigations. Stagnation zone occurs in regions having $\psi \leq 0.3$ while the convective zone is observed at $\psi > 0.3$.

(4) It can be seen that at 0° inclination, convective zone covers the entire surface area of the receiver while the percentage of convective zone is the least at 90° inclination. At inclinations of 30°, 45° and 60°, the receiver surface area covered by the convective zone are 55%, 44% and 28% respectively.

Acknowledgements

The authors wish to thank the Ministry of New and Renewable Energy (MNRE), Government of India for providing the financial assistance to carry out the research work. The help provided by our lab staff for the setting up the experiment is deeply acknowledged.

References

[1] S.B. Kedare, J.K. Nayak, A.D. Paranjape, Development, Installation and Evaluation of Large Scale Concentrating Solar Collector for Medium Temperature Industrial Thermal Applications Final Report of R&D project no. 15/9/2002-ST. Ministry of New and Renewable Energy, Govt. of India, 2006.
[2] J.A. Harris, T.G. Lenz, Thermal performance of solar concentrator/cavity receiver systems. Solar Energy 34 (1985) 135–142.
[3] W.B. Stine, C.G. McDonald, Cavity receiver heat loss measurements, in: Proceedings of ASME Solar Energy Division Conference, Denver, Colorado, 1988.
[4] U. Leibfried, J. Ortjohann, Convective heat loss from upward and downward-facing cavity solar receivers: measurements and calculations. Journal of Solar Energy Engineering 117 (1995) 75–84.
[5] A.M. Clausing, An analysis of convective losses from cavity solar central receivers. Solar Energy 27 (4) (1981) 295–300.
[6] A.M. Clausing, Convective losses from cavity solar receivers – comparisons between analytical predictions and experimental results. Journal of Solar Energy Engineering 105 (1983) 29–33.
[7] P. Le Quere, J.A.C. Humphrey, F.S. Sherman, Numerical calculation of thermally driven two-dimensional unsteady laminar flow in cavities of rectangular cross section. Numerical Heat Transfer 4 (1981) 249–283.
[8] P. Le Quere, F. Penot, M. Mirenayat, Experimental study of heat loss through natural convection from an isothermal cubic open cavity. in: P.K. Falcone (Ed.), Proceedings DOE/SERI/SNLL Workshop on Convective Losses from Solar Receivers (1981), pp. 165–174 Sandia Laboratory Report SAND81-8014, Livermore, California.
[9] F. Penot, Numerical calculation of two-dimensional natural convection in isothermal open cavities. Numerical Heat Transfer 5 (1982) 421–437.
[10] C.F. Hess, R.H. Henze, Experimental investigations of natural convection losses from open cavities. Journal of Heat Transfer 106 (1984) 333–338.
[11] K.S. Chen, J.A.C. Humphrey, F.S. Sherman, Convective flow in a heated cavity – free and mixed convective flow of air in a heated cavity of variable rectangular cross-section and orientation. Philosophical Transactions of the Royal Society of London A316 (1985) 57–84.
[12] Y.L. Chan, C.L. Tien, A numerical study of two-dimensional laminar natural convection in shallow open cavities. International Journal of Heat and Mass Transfer 28 (1985) 603–612.
[13] Y.L. Chan, C.L. Tien, Laminar natural convection in shallow open cavities. Journal of Heat Transfer 108 (1986) 305–309.
[14] M.D. Pavlovic, F. Penot, Experiments in the mixed convection regime in an isothermal open cubic cavity. Experimental Thermal and Fluid Science 4 (1991) 648–655.
[15] H. Skok, S. Ramadhyani, R.J. Schoenhals, Natural convection in side-facing open cavity. International Journal of Heat and Fluid Flow 12 (1991) 36–45.
[16] W. Chakroun, M.M. Elsayed, S.F. Al-Fahed, Experimental measurements of heat transfer coefficient in a partially/fully opened tilted cavity. Journal of Solar Energy Engineering 119 (1997) 298–303.
[17] R.Y. Ma, Wind Effects on Convective Heat Loss from a Cavity Receiver for a Parabolic Concentrating Solar Collector, Sandia National Laboratories Report, SAND92-7293, 1993.
[18] C.G. McDonald, Heat Loss from an Open Cavity, Sandia National Laboratories Report, SAND95-2939, 1995.
[19] L.L. Eyler, Predictions of convective losses from a solar cavity receiver. in: P.K. Falcone (Ed.), Proceedings DOE/SERI/SNLL Workshop on Convective Losses from Solar Receivers (1981), pp. 93–104 Sandia Laboratory Report SAND81-8014, Livermore, California.
[20] N. Sendhil Kumar, K.S. Reddy, Numerical investigation of natural convection heat loss in modified cavity receiver for fuzzy focal solar dish concentrator. Solar Energy 81 (2007) 846–855.
[21] S. Paitoonsurikarn, K. Lovegrove, Numerical investigation of natural convection loss in cavity-type solar receivers, in: Proceedings of Solar 2002, ANZSES Annual Conference, Newcastle, Australia, 2002.
[22] S. Paitoonsurikarn, K. Lovegrove, On the study of convection loss from open cavity receivers in solar paraboloidal dish application, in: Proceedings of Solar 2003, ANZSES Annual Conference, Melbourne, Australia, 2003.
[23] S. Paitoonsurikarn, T. Taumoefolau, K. Lovegrove, Estimation of convection loss from paraboloidal dish cavity receivers, in: Proceedings of Solar 2004: Life, the Universe and Renewables, 42nd Annual Conference of the Australian and New Zealand Solar Energy Society, Perth, Australia, 2004.
[24] K.S. Reddy, N. Sendhil Kumar, Combined laminar natural convection and surface radiation heat transfer in a modified cavity receiver of solar parabolic dish. International Journal of Thermal Sciences 47 (2008) 1647–1657.
[25] N. Sendhil Kumar, K.S. Reddy, Comparison of receivers for solar dish collector system. Energy Conversion and Management 49 (2008) 812–819.
[26] Fluent Inc., copyright, CFD software package, 2003.
[27] J.P. Holman, Heat Transfer, Eighth SI Metric Edition. Tata McGraw-Hill Publishing Company Limited, New Delhi, 2002.
[28] D.D. Gray, A. Giorgini, The validity of the Boussinesq approximation for liquids and gases. International Journal of Heat and Mass Transfer 19 (1976) 545–551.
[29] M. Prakash, S.B. Kedare, J.K. Nayak, Investigations on heat losses from a solar cavity receiver. Solar Energy 83 (2009) 157–170.